
Article:
Liu, Y., Huang, S.-S. and Burgess, I. (2020) Performance of a novel ductile connection in steel-framed structures under fire conditions. Journal of Constructional Steel Research, 169. 106034. ISSN 0143-974X

https://doi.org/10.1016/j.jcsr.2020.106034

Performance of a novel ductile connection in steel-framed structures under fire conditions

Yu Liu[1*], Shan-Shan Huang[1] and Ian Burgess[1]

[1] Department of Civil and Structural Engineering, University of Sheffield, Mappin Street, Sheffield S1 3JD, United Kingdom.

* Corresponding Author: E-mail address: yliu230@sheffield.ac.uk (Yu Liu)

Abstract

The component-based model of a novel connection, which is designed to accommodate the high ductility demand of long-span steel beams in fire conditions, has been incorporated into the finite element software Vulcan. A single beam with the novel connections connecting it to rigid supports at both ends is first used to verify that the component-based model has been correctly incorporated into Vulcan, by comparing its results with those from detailed finite element models using the general-purpose package Abaqus. The performance of the novel connection has been compared with that of conventional connection types, including ideally rigid and pinned connections, end-plate and web-cleat connections, using a sub-frame model. Results show that, compared with other connection types, the novel connection provides much higher axial and rotational ductilities, to accommodate the deformations generated by the connected beam as its temperature rises. To optimize the performance of the novel connection under the tensile axial forces generated by the eventual catenary action of heated, unprotected beams at high temperatures, parametric studies have been carried out on the influence of four key parameters, including the temperature of the connection, the inner radius of its semi-cylindrical section, the plate thickness and the bolt spacing. It is found that it is possible to optimize connection thickness, protection level, and inner radius of the semi-cylindrical section in order to delay the occurrence of bolt pull-out failure, and thus enhance a beam's ultimate failure temperature. Finally, the combined static-dynamic solver of Vulcan is used to simulate the progressive collapse of a three-storey, three-bay frame with these novel connections. This progressive collapse simulation emphasizes the importance of connections for the survival of the entire structure in a fire event.

Keywords: Ductility, Connections, Fire, Vulcan, Progressive collapse

1. Introduction

Connection failures observed in the collapse of The World Trade Centre [1], as well as in the Cardington full-scale fire tests [2], indicated that connections are potentially the weakest part of a steel-framed structure in a fire event. Connections play a key role in maintaining the integrity of a structure, and can prevent progressive collapse by tying different structural components together. The behaviour of connections at elevated temperatures is quite different from that at ambient temperature. The internal forces experienced by connections change, from a combination of shear and axial compressive force due to restraint of the thermal expansion of beams in the initial stage of a fire, to tensile force caused by the eventual catenary action of beams at very high temperatures. However, conventional connection types lack the ductility to accommodate either the compressive or tensile movements, and this can result in fracture of the connection. Once such a fracture occurs, the connected beam detaches from the supporting column, which can lead to an increased column slenderness ratio and thus to potential column buckling. Connection failures can also trigger the collapse of the supported slab, leading to the spread of fire into adjacent compartments. In order to provide the beam-column connection with high ductility, a novel connection has been proposed by the authors in the previous papers [3-5]. This novel connection can be considered as an angle-cleat with greatly enhanced ductility. The connection piece is formed from a single plate, and consists of two identical parts, each of which takes the form of a fin-plate which is bolted to the beam web, an end-plate which is bolted to either the column web or flange, with a semi-cylindrical section between the fin-plate and end-plate. The semi-cylindrical section provides the additional axial ductility by bending, thus allowing the fin-plate to move towards or away from the end-plate. Analytical models of the novel connection have been proposed, based on simple plastic theory. These were validated against both Abaqus simulations and experiments [3]. A structural sub-frame model, analysed using Abaqus, was used to compare the performance of the novel connection with that of the normal web-cleat connection [4]. The results showed that the axial force generated in the beam with the novel connections was significantly reduced due to the high axial ductility created. This showed well the effect of axial ductility of the novel connection, which accommodates the deformation of the connected beam in fire conditions, reducing the axial forces compared with those in the web-cleat connection.

As mentioned above, forces applied to connections in fire are complicated. Therefore, it is difficult to reproduce such complex loading conditions in experiments, other than in full-scale tests. Compared with experiments, numerical modelling is a more feasible and inexpensive method to investigate the behaviour of connections under

the combined action of material degradation and complex internal forces. The finite element method is a reliable technique which enables prediction of the behaviour of connections in a very detailed manner. Yu [6] used the explicit dynamic solver of Abaqus to analyse bolted steel connections, because the large numbers of contact conditions in the model would cause computational problems for a conventional implicit solver. Sarraj [7] used Abaqus to build a highly detailed three-dimensional finite element model of a fin-plate connection which accounts for material and geometric non-linearity, large deformations and contact behaviour. Elsawaf [8] also used Abaqus to model the behaviour of restrained structural subassemblies incorporating a steel beam and concrete-filled tubular (CFT) columns, connected using reverse channel connections in fire. However, such detailed finite element approaches are not suitable in practical fire engineering design, because of the time-consuming nature of model building and computational costs, particularly where global frame analysis needs to be carried out. An alternative way of conducting large-scale frame analysis in fire is to use the component-based method to simulate connection behaviour in structural frame analysis software. The concept of the component-based method, which was initially used to describe the moment-rotation behaviour of steel-to-steel connections at ambient temperature, was first proposed in the 1980s [9] and subsequently adopted in design guidance [10]. Compared with detailed finite element modelling, the component-based method is a good compromise between accuracy and computational efficiency, and it has therefore become popular in recent years. This method is to divide each connection into basic components, such as the end-plate, the beam web, the column flange, the column web, bolts, washers, etc. Each component is idealized as a spring of known stiffness and strength. Jaspart [11] has summarized the three principal steps of component-based modelling as: identification of active components, evaluation of the mechanical properties of each component, and assembly of the active components. Leston-Jones [12] used components representing the column flange in bending, bolts in tension, end-plate in bending and column web in compression to build his spring model for the flush end-plate connection, and this model was validated against his experiments. Block [13] proposed a component-based model for end-plate connections based on the analytical model of a T-stub developed by Spyrou [14]. Continuing his work, Dong [15, 16] further extended the connection element types in Vulcan, and developed a user-defined connection element, a flush end-plate connection element and a reverse channel connection element. Taib [17] used two basic components, the plate in bearing and the bolt in shear, to model the fin-plate connection. The component-based model of the novel connection was proposed by the authors in a previous paper [5]. The analytical model of the "web-cleat" component of the novel connection, and the web-cleat/semi-cylindrical (WCSC) component, in which the semi-cylindrical component and the web-cleat component are considered to deform as a

whole, on the basis of simple plastic theory, were developed. Based on these, two component-based models for the novel connection were proposed, and the results of the two component-based models were compared and validated against both Abaqus simulations and experiments. In general, the results from the second (WCSC) component-based model were seen to be the more accurate, and therefore this is now incorporated into the software Vulcan for global frame analysis.

The software Vulcan [18-20] developed by the Structural Fire Engineering Research Group at the University of Sheffield is able to carry out 3D modelling and robustness assessment of structures in fire. In order to simulate the complete behaviour of a structure in fire, from local instability to final collapse, Sun [21-23] developed a procedure which combined static and dynamic solvers to make full use of the advantages of each. In this way, Vulcan can use its static solver to simulate the static behaviour of the structure until instability occurs, at which stage the dynamic solver is activated to track the motion of the structure until stability is regained. Combining this with the parallel development of component-based connection models, Vulcan is capable of tracking the behaviour of connections from initial movement, through the fracture of individual components, to eventual failure.

This research aims to incorporate the component-based model of the novel connection into Vulcan. The analytical model of bolt pull-out has been added to the component-based model [5]. The tangent stiffness matrix derived by Block [13] has been used to convert the component-based model of the novel connection into a connection element, following the principles of the finite element method. A single beam model with these connections at each end has been modelled using both Vulcan and Abaqus, in order to establish whether the component-based model in Vulcan adequately represents the behaviour shown by a detailed FE analysis. Sub-frame models have also been created in order to compare the performance of the novel connection with that of conventional connection types. Different types of connections are used in these sub-frame models including idealised rigid and pinned connections, and the commonly-used end-plate and web-cleat connection types. In order to model the web-cleat connection using Vulcan, the analytical model developed by Yu [24], has been implemented in the software in the same way as the new element. Parametric studies have been carried out, in order to optimize the performance of the novel connection under the tensile axial forces generated by the eventual catenary action of unprotected beams at high temperatures. Four key parameters including the temperature of the connection, the inner radius of its semi-cylindrical section, the plate thickness and the bolt spacing are selected. Finally, the static-dynamic solver has been used to simulate the progressive collapse of a three-storey three-bay plane frame using the novel connections.

2. Incorporation of the component-based model into Vulcan

The novel ductile connection proposed by the authors in previous papers [3-5] is shown in Figure 1. It consists of two identical parts, each of which includes a fin-plate, a semi-cylindrical section and a web-cleat.

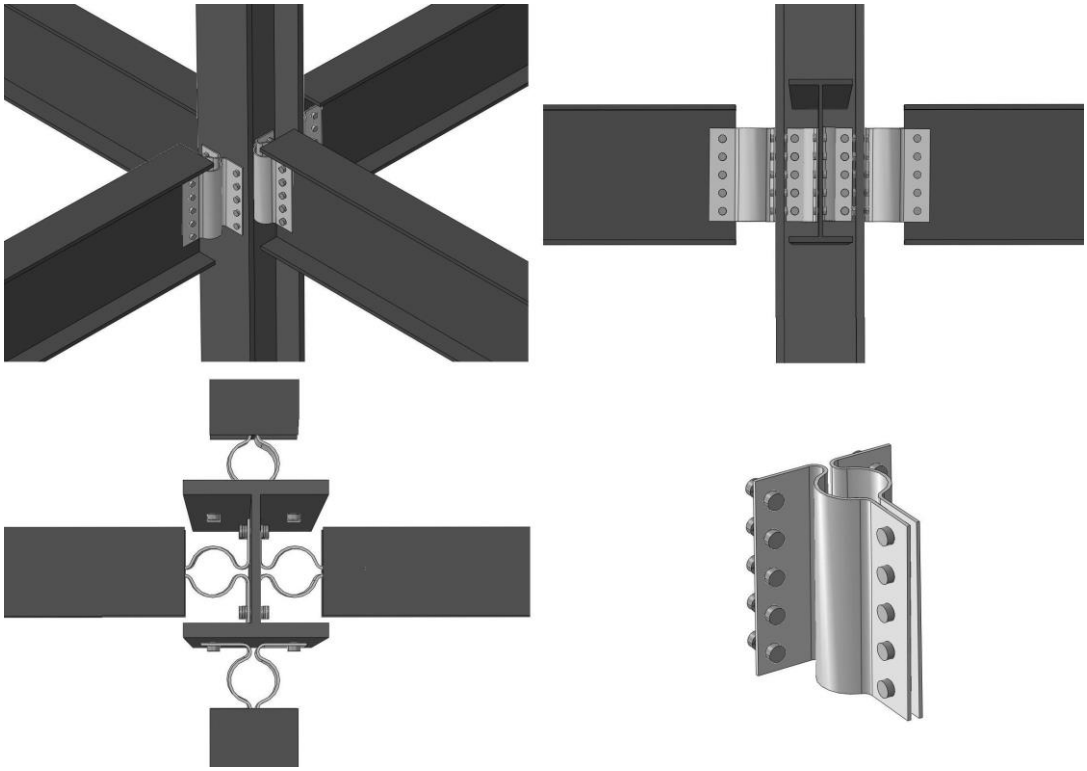

Figure 1. The proposed novel connection

The semi-cylindrical section is the key component, providing additional ductility by allowing the fin-plate to move towards and away from the column flange. To integrate the component-based model, shown in Figure 2, of the connection into global frame analysis, the component-based model needs to be converted into a connection element and then incorporated into Vulcan. The component-based model proposed in the previous paper [5] includes the behaviour modes associated with fin-plate connections (bolt and plate shear and bearing), and those of the semi-cylindrical section (plastic bending and tensile fracture). However, the detailed Abaqus simulations show that bolt pull-out failure from the web-cleat zone may be the most critical failure mode in practical designs. Therefore, a simplified model of bolt pull-out failure has been added to each spring row (bolt row) of the component-based model as a separate component, before converting the whole component-based model into a connection element and incorporating it into Vulcan.

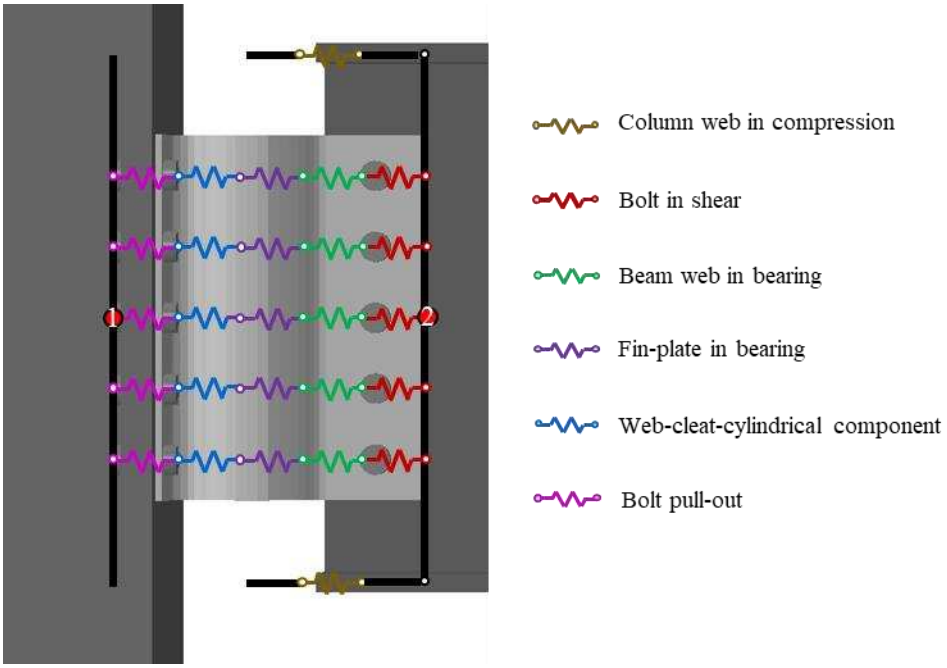

Figure 2. Component-based model of the novel connection

2.1 Analytical model of bolt pull-out failure

Dong [16] developed a simplified 'plastic cone' model to calculate the local deformation of steel plate around a bolt hole during pull-out, as shown in Figure 3. According to the virtual work principle, the external work done by the bolt tensile force F in a vertical displacement increment $d\delta$, should be equal to the increment of internal absorbed work dW_{total}, which includes increments of the plastic work in the circular plastic hinge $dW_{circular}$ and the plastic work induced by circumferential stretching of the cone wall dW_{strip} (Equation (1)). The contact between the bolt head and steel plate in the 'cone' model is considered by determining the deformation of the cone wall according to the position and the diameter of the bolt head, as shown in Figure 3. However, the proposed 'cone' model is just a simplified way to incorporate the bolt pull-out failure into the component-based model of the novel connection. Therefore, the effects of stress concentration, cracking of the steel plate around the bolt hole and the complex contact between the bolt head edge and the steel plate when the steel plate is under partial bending and partial tension are neglected. Equations (2)-(7) derived by Dong are adapted here to generate the F-δ curve of the bolt pull out component. The plastic work induced by stretching of the cone wall at a given bolt head movement δ can be calculated using Equation (2) according to the relationship between ΔL_{strip}, ΔL_y and ΔL_u. The rotation θ of the cone wall relative to its original position, is calculated using Equation (3) and shown in Figure 3. ΔL_{strip} is the

average elongation of the cone wall circumference and is given in Equation (4). ΔL_y and ΔL_u are the elongation of the cone wall under yield load and ultimate load, respectively, which can be calculated using Equation (5). Equations (6) and (7) are used to calculate the increment of internal absorbed work dW_{total}, maximum movement of bolt head $\delta_{\max}$ and maximum rotation of the cone wall $\theta_{\max}$, respectively. The F-δ curves of the other components are obtained using the analytical models developed in the previous papers [3, 5]. The revised component-based model of the novel connection is shown in Figure 2. The gaps included in the compression spring rows at the upper and lower beam flanges represent the maximum clearance between these flanges and the column-face before contact occurs. Since the vertical shear behaviour has not been taken into consideration, the component-based model is assumed to be rigid in the vertical direction. The loading and unloading behaviour have been incorporated into the individual component characteristics, to enable simulation of the complicated loading conditions experienced by the connection under fire conditions.

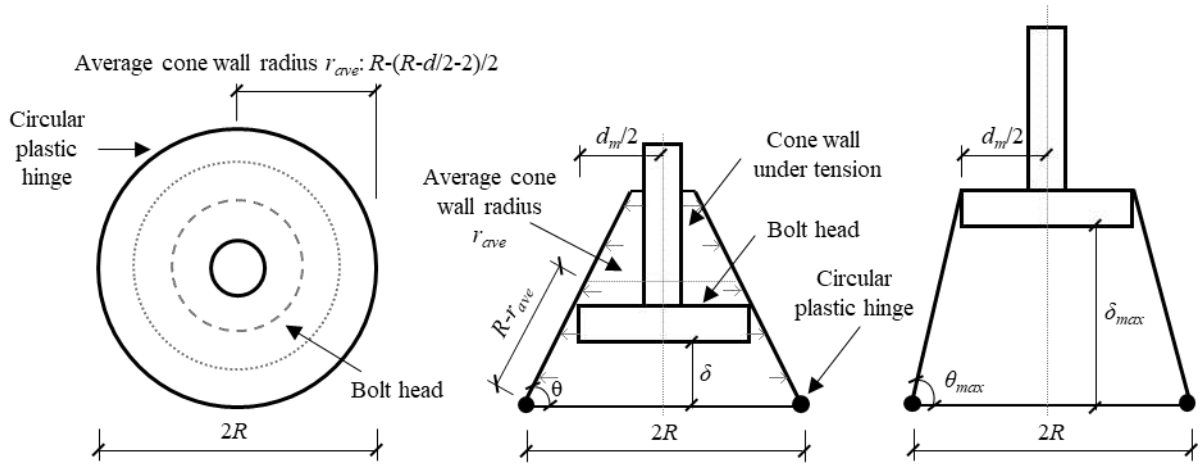

Figure 3. Simplified 'cone' model

$$F = dW_{total} \,/\, d\delta = d\left(W_{strip} + W_{circular}\right) / d\delta \tag{1}$$

$$dW_{strip} = \begin{cases} \dfrac{EA}{L_{strip}} \Delta L_{strip} \cdot d\left(\Delta L_{strip}\right) & \Delta L_{strip} \le \Delta L_y \\ f_y A \cdot d\left(\Delta L_{strip}\right) + \dfrac{E_T A}{L_{strip}} \left(\Delta L_{strip} - \Delta L_y\right) \cdot d\left(\Delta L_{strip}\right) & \Delta L_y < \Delta L_{strip} \le \Delta L_u \\ f_u A \cdot d\left(\Delta L_{strip}\right) & \Delta L_{strip} > \Delta L_u \end{cases} \tag{2}$$

$$\theta = \arctan\left(\frac{\delta}{R - d_m / 2}\right), \quad d\theta = \frac{d\delta}{\left[1 + \left(\frac{\delta}{R - d_m / 2}\right)^2\right](R - d_m / 2)} \tag{3}$$

$$\Delta L_{strip} = 2\pi\left[R - (R - r_{ave})\cos\theta\right] - L_{strip}, \quad d\Delta L_{strip} = 2\pi(R - r_{ave})\sin\theta \cdot d\theta \tag{4}$$

$$\Delta L_y = \frac{f_y L_{strip}}{E}, \quad \Delta L_u = \frac{f_y L_{strip}}{E} + \frac{(f_u - f_y) L_{strip}}{E_T} \tag{5}$$

$$dW_{circular} = M_p \times 2\pi R \times d\theta = \left(\frac{f_y t^2}{4}\right) \frac{d\delta}{\left[1 + \left(\frac{\delta}{R - d_m / 2}\right)^2\right](R - d_m / 2)} \tag{6}$$

$$\theta_{\max} = \arccos\left((R - d_m / 2) / (R - d / 2 - 2)\right), \quad \delta_{\max} = (R - d / 2 - 2)\sin\theta_{\max} \tag{7}$$

in which d is the initial diameter of the bolt hole, $r_{ave} = R - \left[R - (d / 2 + 2)\right] / 2$ is the average radius of the cone wall, $L_{strip} = 2\pi r_{ave}$ is the average circumference of the cone wall, A is the average cross-sectional area of the cone wall, t is the thickness of the cone wall.

2.2 Incorporation into Vulcan

The existing subroutine SEMIJO of Vulcan was originally specified for simple spring elements, including rigid, pinned and semi-rigid connections. This subroutine passes the incremental displacement vector to the connection element and returns the tangent stiffness matrix and force vector to the main program. The properties of the novel connection element developed in this paper are accessible to this subroutine, which was also used by Block [13] and Dong [16] for their connection elements. Following the principles of the finite element method, the tangent stiffness matrix derived by Block [13], represented by Equations (8) and (9), is adopted here to convert the component-based model of the novel connection into a connection element. The symbols i and j in Equation (8) represent the two end nodes of the connection element. During the calculation process, Vulcan provides an incremental displacement of the connection element based on the previous step's stiffness, and then the tangent stiffness matrix is recalculated and the incremental force vector is updated. The updated tangent stiffness matrix and the incremental force vector are returned back to the main program. A convergence check based on out-of-balance forces is carried out to determine whether either the next load or temperature step will be applied to the model or the current load step should be reduced until the convergence criteria are satisfied. As shown in Equation

(8), the out-of-plane and torsional DoFs are assumed to be connected rigidly and without interaction, since they are in any case of relatively minor importance in steel structures.

$$K_{Connection} = \begin{array}{c} \\ i \\ \\ \\ \\ \\ \\ j \\ \\ \\ \\ \\ \end{array} \begin{array}{c} \begin{array}{cccccc} i & & & & & \end{array} \\ \begin{array}{cccccc} U & V & W & R_X & R_Y & R_Z \end{array} \\ \begin{pmatrix} K_{11} & 0 & 0 & 0 & K_{15} & 0 \\ 0 & \infty & 0 & 0 & 0 & 0 \\ 0 & 0 & K_{33} & 0 & 0 & 0 \\ 0 & 0 & 0 & \infty & 0 & 0 \\ K_{51} & 0 & 0 & 0 & K_{55} & 0 \\ 0 & 0 & 0 & 0 & 0 & \infty \\ -K_{11} & 0 & 0 & 0 & -K_{15} & 0 \\ 0 & -\infty & 0 & 0 & 0 & 0 \\ 0 & 0 & -K_{33} & 0 & 0 & 0 \\ 0 & 0 & 0 & -\infty & 0 & 0 \\ -K_{51} & 0 & 0 & 0 & -K_{55} & 0 \\ 0 & 0 & 0 & 0 & 0 & -\infty \end{pmatrix} \end{array} \begin{array}{c} \begin{array}{cccccc} & & & & & j \end{array} \\ \begin{array}{cccccc} U & V & W & R_X & R_Y & R_Z \end{array} \\ \begin{pmatrix} -K_{11} & 0 & 0 & 0 & -K_{15} & 0 \\ 0 & -\infty & 0 & 0 & 0 & 0 \\ 0 & 0 & -K_{33} & 0 & 0 & 0 \\ 0 & 0 & 0 & -\infty & 0 & 0 \\ -K_{51} & 0 & 0 & 0 & -K_{55} & 0 \\ 0 & 0 & 0 & 0 & 0 & -\infty \\ K_{11} & 0 & 0 & 0 & K_{15} & 0 \\ 0 & \infty & 0 & 0 & 0 & 0 \\ 0 & 0 & K_{33} & 0 & 0 & 0 \\ 0 & 0 & 0 & \infty & 0 & 0 \\ K_{51} & 0 & 0 & 0 & K_{55} & 0 \\ 0 & 0 & 0 & 0 & 0 & \infty \end{pmatrix} \end{array} \begin{array}{c} \\ U \\ V \\ W \\ R_X \\ R_Y \\ R_Z \\ U \\ V \\ W \\ R_X \\ R_Y \\ R_Z \end{array} \tag{8}$$

in which

$$K_{11} = \sum_{i=1}^{n} k_{T,i} + \sum_{i=1}^{2} k_{C,i}\ , \quad K_{15} = K_{51} = \sum_{i=1}^{n} k_{T,i} \cdot l_{T,i} + \sum_{i=1}^{2} k_{C,i} \cdot l_{C,i}\ , \quad K_{33} = k_s\ , \quad K_{55} = \sum_{i=1}^{n} k_{T,i} \cdot l_{T,i}^2 + \sum_{i=1}^{2} k_{C,i} \cdot l_{C,i}^2 \tag{9}$$

in which the subscripts T, C and S represent the springs working in tension, compression and shear respectively, and n is the number of bolt rows. $k_{T,i}$ / $k_{C,i}$ represents the stiffness of ith tension/compression spring row. $l_{T,i}$ / $l_{C,i}$ represents the lever arm of the ith tension/compression spring row to the centre of rotation.

3. Validation of the connection element against Abaqus

In order to verify whether the connection element in Vulcan adequately represents the behaviour shown by a detailed FE analysis, a single beam of length 7.5 m (Figure 4), with novel connections at both ends, is modelled using both Vulcan and Abaqus. It is difficult to verify the Abaqus single-beam model with connections at beam ends, therefore, therefore, the verifications of the beam and connection parts of the model were conducted separately. The connection part of the Abaqus model has been validated against push/pull experiments on model-scale specimens [3, 5] and a good agreement between the test and modelling results were obtained. The beam part of the model was checked against hand calculations of a simply supported beam under increasing UDL at various temperatures (20 °C and 500°C). The comparison results are shown in Figure 5, indicating that the Abaqus results have a good correlation with the hand calculations before inelasticity.

A uniformly distributed line load of 42.67 kN/m is applied to the single beam model, generating a load ratio of 0.4 with respect to a simply supported beam. It is assumed that there are three cases, in which the temperatures of the connections are equal to 20℃, and then 50% and 100% of the temperature of the connected beam, respectively, as shown in Figure 4. Comparisons between results from Vulcan and Abaqus are shown in Figure 6, Figure 7 and Figure 8 for the three case. It is obvious that the ultimate failure temperature of the connection decreases with the increase of connection temperature relative to that of the beam, as expected. As shown in Figure 6 (a), Figure 7 (a) and Figure 8 (a), the mid-span deflection of the Vulcan model increases rapidly after 500℃, until the slope of the deflection-temperature curve is nearly vertical, at around 845℃, 768℃ and 664℃ respectively, indicating the failure of the connection by bolt pull-out. The connected beam then detaches from the column and loses its axial constraint. This is shown by the rapid decreases of the axial tensile forces at around 845℃, 768℃ and 664℃ in Figure 6 (b), Figure 7 (b) and Figure 8 (b). The failure temperatures predicted by Abaqus in Cases 2 and 3 are higher than those predicted by Vulcan. This is because fracture criteria are not set in the Abaqus models, resulting in unreasonably large deformation rather than fracture. The failure modes of the three cases modelled in Vulcan are all bolt pull-out failures, which are consistent with the simulation results of Abaqus, as shown in Figure 9. Except for the final failure stage, the deflection and the axial force predicted by Vulcan are very close to those given by Abaqus, indicating that the novel connection element adequately represents the behaviour of the connection.

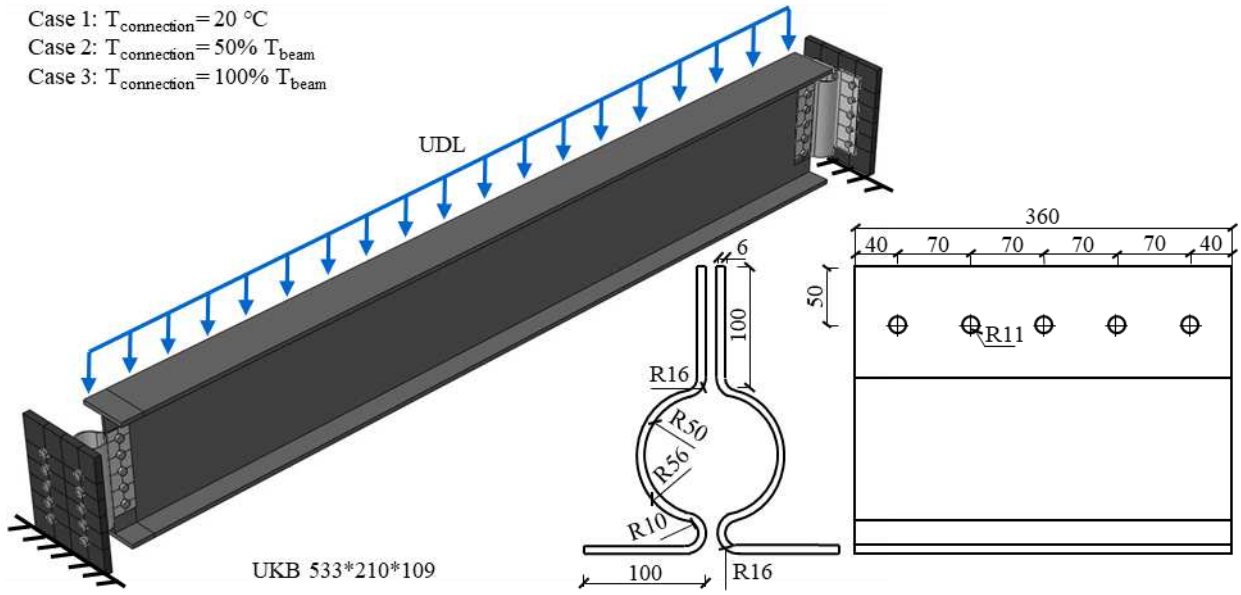

Figure 4. Single beam model

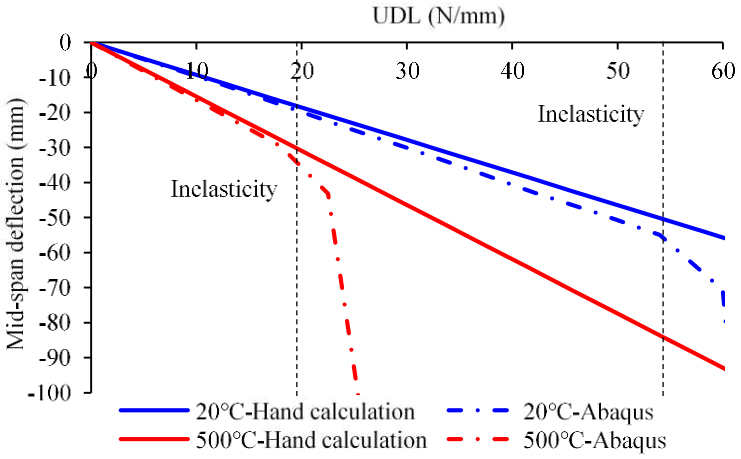

Figure 5 Comparison between Abaqus results and hand calculation results

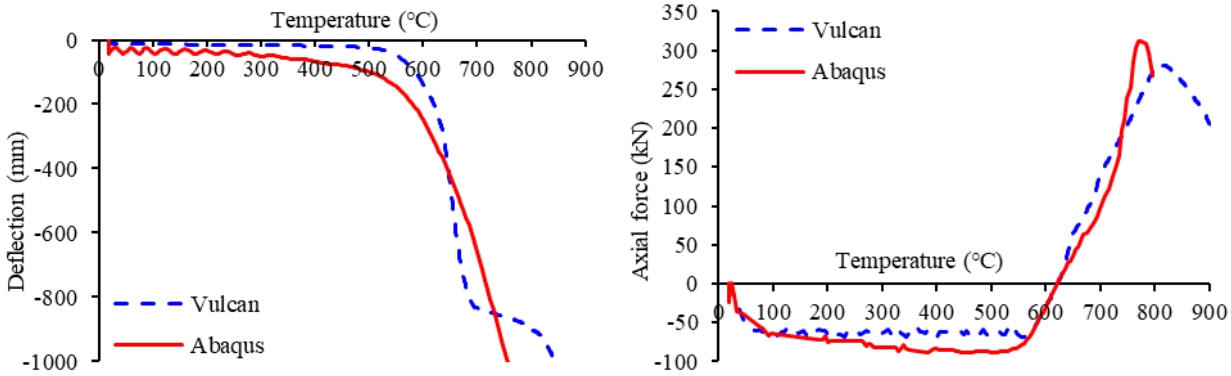

(a) Mid-span deflection of beam (b) Axial force of beam

Figure 6. Comparison results of Case 1

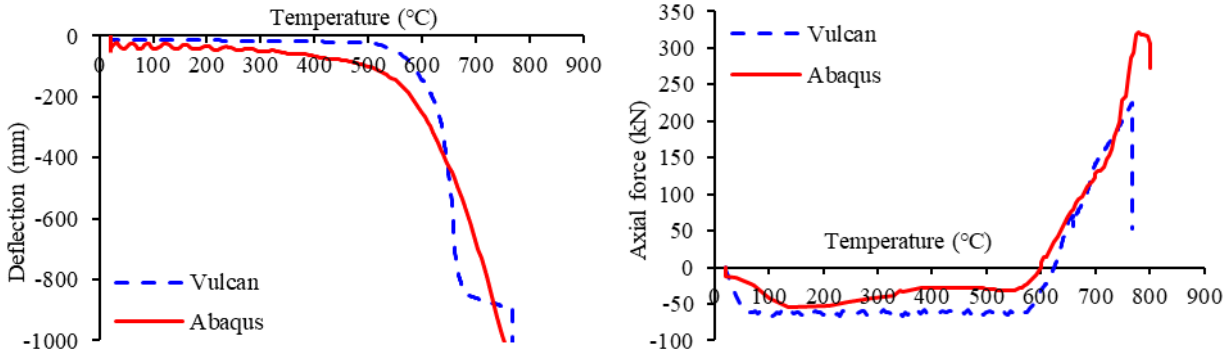

(a) Mid-span deflection of beam (b) Axial force of beam

Figure 7. Comparison results of Case 2

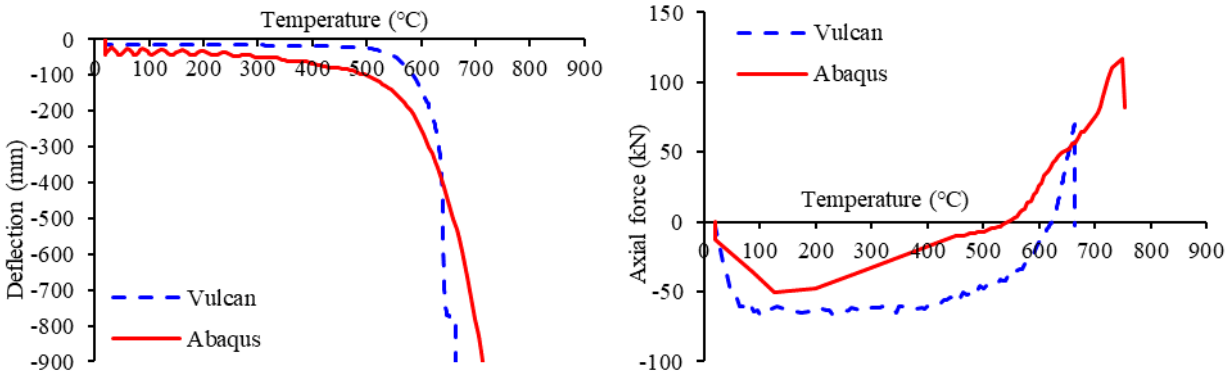

(a) Mid-span deflection of beam (b) Axial force of beam

Figure 8. Comparison results of Case 3

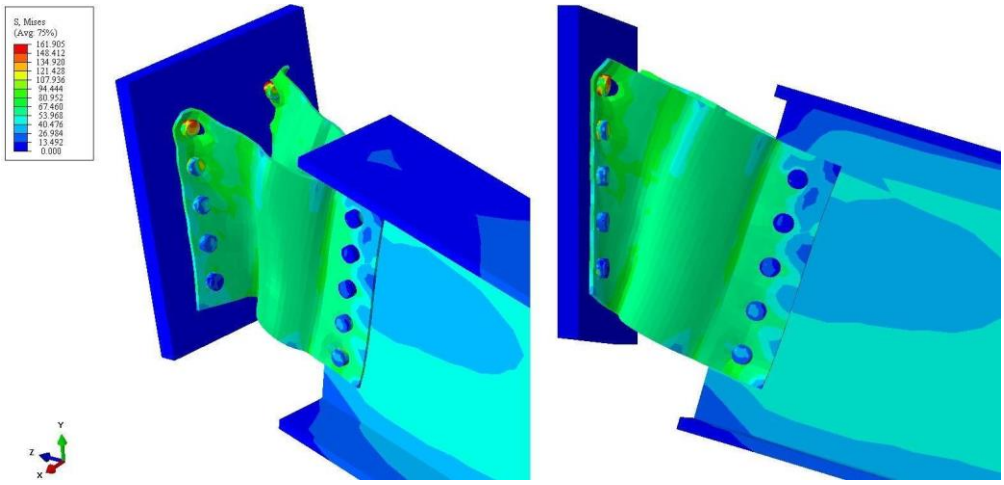

Figure 9. Bolt pull-out failure

Figure 10, Figure 11 (a) and Figure 12 (a) show the force-displacement curves of each spring row. It can be seen that each spring row will undergo different stages as the connection deforms; pushing, unloading of pushing, pulling-back and finally pulling. During the pulling-back stage, a spring row is pulled back to its original state after compressive deformation. In Case 3, since the temperature of the connection is equal to that of the connected beam, the temperature of the connection reaches nearly 600℃ before it enters the pulling-back stage. The mechanical properties of steel degrade rapidly after 400℃, which leads to the decrease of compressive forces shown in Figure 12 (a). The force-temperature curves of each spring row in Cases 2 and 3 are shown in Figure 11 (b) and Figure 12 (b). As expected, the evolution of the axial force of each spring row almost corresponds to the beam's axial force development. In the initial stage of heating, each spring row is subjected to compressive force, due to restraint of the thermal expansion of the connected beam. When the temperature of beam exceeds 600℃, it enters the catenary action phase, and the force of all spring rows becomes tensile. After the deformation limit is reached, the tensile

force of each spring row increases rapidly in a pure tension mechanism. Since the failure temperature of the connection in Case 2, which is around 760°C, is higher than that in Case 3, which is around 660°C, the ultimate tensile force of each spring row in Case 2 is higher than that of the corresponding row in Case 3.

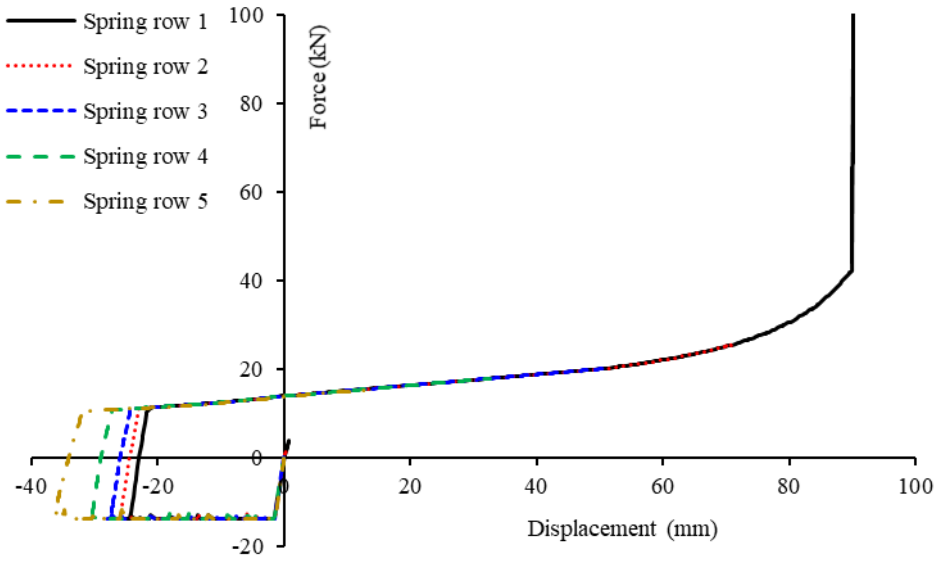

Figure 10. Force-displacement curves of each spring row of the novel connection in Case 1

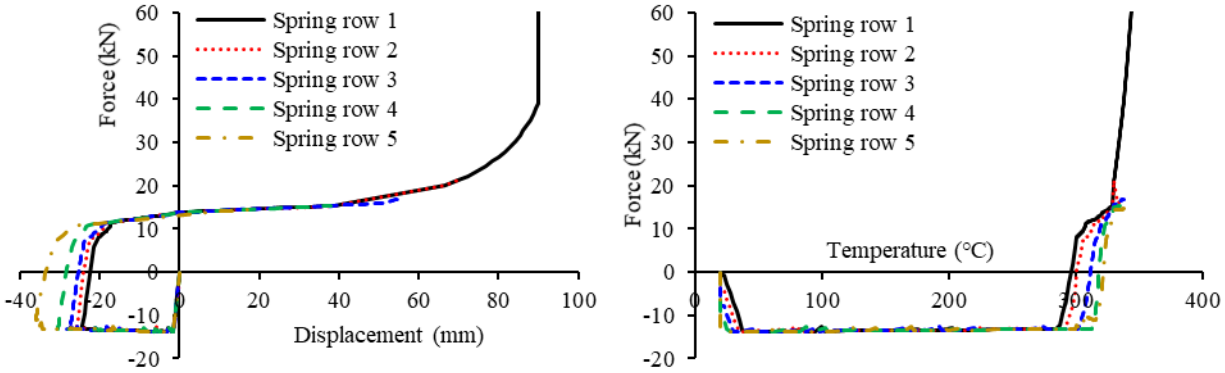

(a) Force-displacement curves (b) Force-temperature curves

Figure 11. Results for each spring row of the novel connection in Case 2

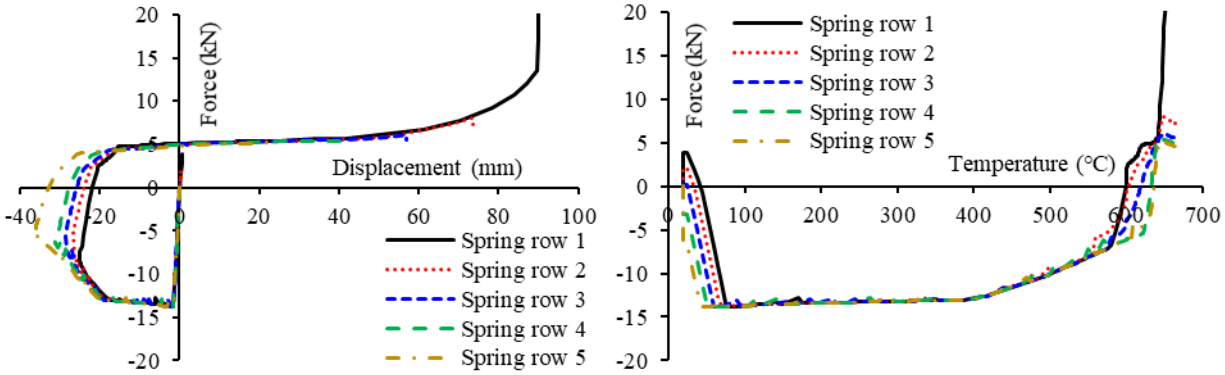

(a) Force-displacement curves (b) Force-temperature curves

Figure 12. Results for each spring row of the novel connection in Case 3

4. Comparison of the novel connection with conventional connection types

The motive behind introducing the novel connection is to enhance the ductility of connections, so as to accommodate the large deformations generated by the connected beams as their temperatures rise, in order to improve their robustness in fire. To compare the performance of this new connection type with that of conventional connection types, a sub-frame model, shown in Figure 13 (a), is used. It is assumed that the connections and the columns in the first floor are protected to the same level, therefore the column temperature and connection temperature are both set to 50% of the unprotected beam temperature. Different types of connection have been used in this sub-frame model, including idealised rigid and pinned connections, as well as the commonly-used end-plate and web-cleat connections. An end-plate connection element has already been incorporated into Vulcan by Block [13] and Dong [16]. Although the Structural Fire Engineering Research Group at the University of Sheffield has done some research on web-cleat connections, including experiments [25] and the derivation of analytical models [24], the web-cleat connection had not yet been incorporated into Vulcan. The web-cleat connection has been implemented in Vulcan in this work.

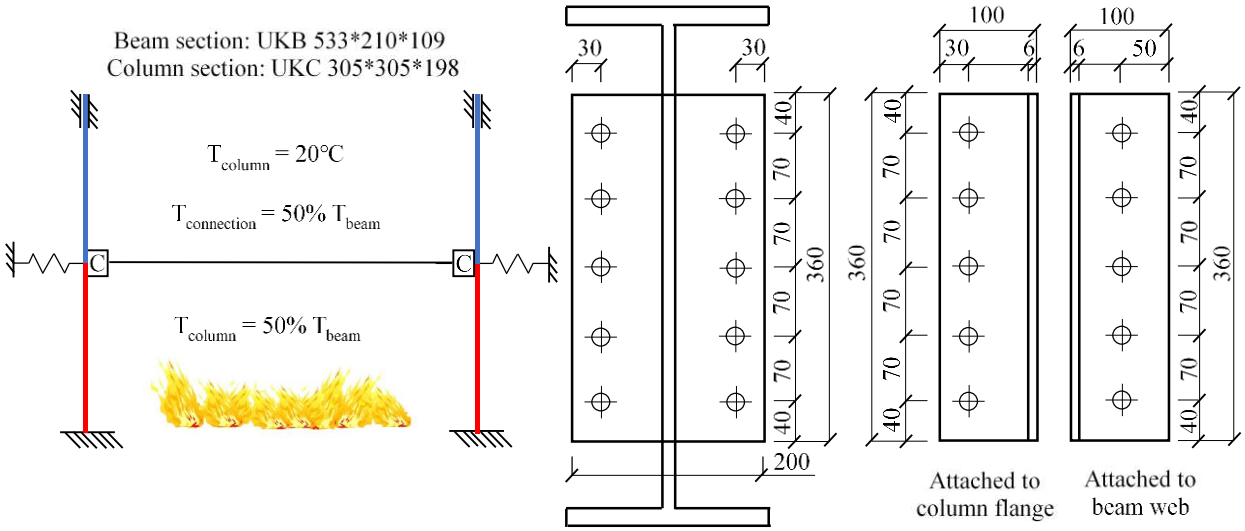

(a) Sub-frame model (b) End-plate connection (c) Web-cleat connection

16a

Figure 13. The sub-frame model

4.1 Integration of web-cleat connection element into Vulcan

During the process of developing the mechanical model of a web-cleat connection, Yu [24] made three assumptions: (i) the two legs of the web-cleat are considered as two orthogonal cantilever beams connected at the middle of the heel with concentrated forces at their ends; (ii) the bolts attached to the column flange can provide full fixity; and (iii) the bolts connected to the beam web allow movement in the plane of the web, as shown in Figure 14 (a). Plastic hinges are formed at the ends of Beams 1 and 2. Depending on the relative relationships between the moments M_{r1} and M_{r2} (Figure 14 (a)) at the beam ends with M_y (yield moment capacity of the plastic hinge) and M_u (ultimate moment capacity of the plastic hinge), the state of the plastic hinge can be divided into five stages. The forces and deformations of the web-cleat are then derived differently depending on the current stage.

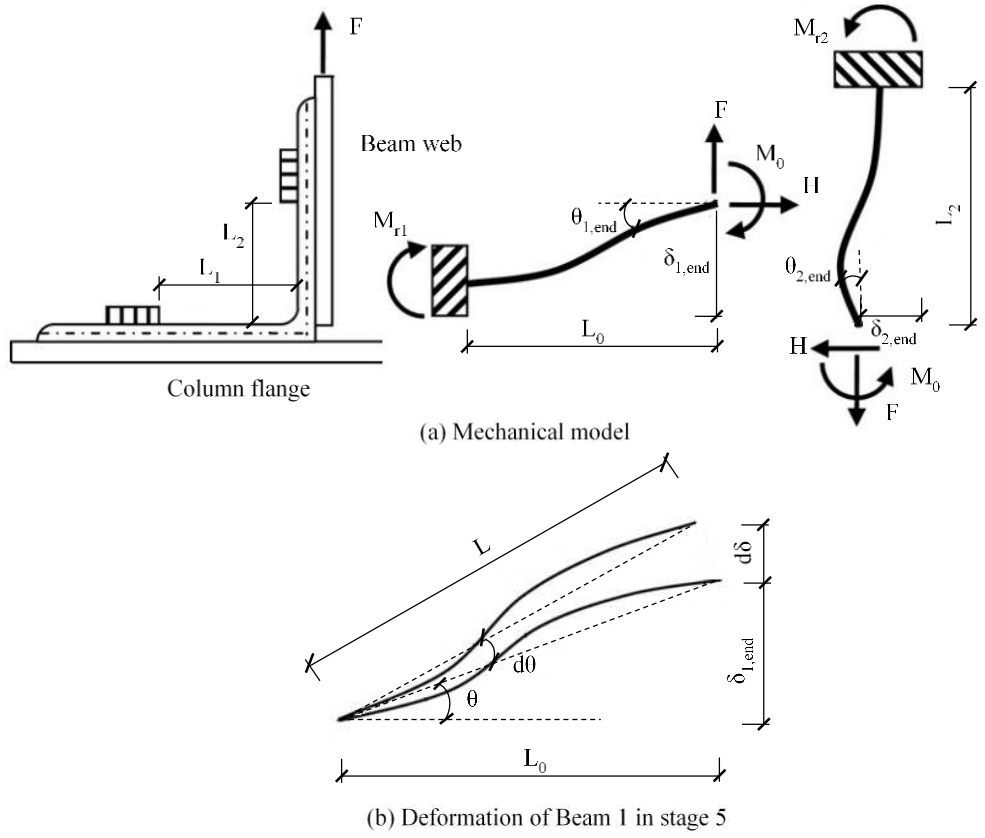

Figure 14. The model of web-cleat connection

Stage 1: ($M_{r1} \le M_y$)

$$M_y = \frac{wt^2 f_y}{4}, \quad M_u = \frac{wt^2 f_u}{4} \tag{10}$$

$$L_1 = L_0 + \frac{1}{2(EI)^2}\left[\frac{1}{20}F^2 L_0^5 - \frac{F}{4}(FL_0 - M_0)L_0^4 + \frac{1}{3}(FL_0 - M_0)^2 L_0^3\right] \tag{11}$$

$$M_0 = \frac{(L_1 - L_0)EI + FL_0^2 L_2 / 3}{L_2^2 / 6 + 2L_0 L_2 / 3} \tag{12}$$

$$\delta_{1,end} = \frac{FL_0^3 / 3 - M_0 L_0^2 / 2}{EI} \tag{13}$$

in which w and t are respectively the effective width and the thickness of the web-cleat. The meanings of the other parameters in these equations are shown in Figure 14 (a). At any applied external force F, L_0 can be found iteratively after substituting Equation (12) into Equation (11). Once L_0 is obtained, M_0 and the vertical displacement $\delta_{1,end}$ at the end of Beam 1 can be obtained from Equations (12) and (13), respectively.

Stage 2: ($M_y < M_{r1} \le M_u$ and $M_0 \le M_y$)

At this stage, the external force F increases by a small amount ΔF in each step, and M_0 is used as the controlling incremental parameter. The value of L_0 from the previous step is used as the initial value for each step; it is then updated at the end of the step using Equation (17). C_1 is a variable used to simplify Equation (17), and is calculated using Equation (16). Once F, C_1 and L_0 are known, the vertical deformation $\delta_{1,end}$ can be obtained using Equation (18).

$$H = \frac{3EI(L_1 - L_0) + 3M_0 L_2^2 / 2}{L_2^3} \tag{14}$$

$$F = \frac{M_0 + M_y - HM_0 L_2^2 / (2EI) + (K_r + HL_0)\left[M_0(L_0 + L_2) - HL_2^2 / 2\right] / (EI)}{L_0 - HL_0^3 / (3EI) + L_0^2 (K_r + HL_0) / (2EI)} \tag{15}$$

$$C_1 = M_0(L_0 + L_2) - \frac{1}{2} FL_0^2 - \frac{1}{2} HL_2^2 \tag{16}$$

$$L_1 - L_0 = \frac{2F^2 L_0^5 / 15 - 5FM_0 L_0^4 / 12 + (M_0^2 + 2FC_1)L_0^3 / 3 - M_0 C_1 L_0^2 + C_1^2 L_0}{2(EI)^2} \tag{17}$$

$$\delta_{1,end} = \frac{FL_0^3 / 3 - M_0 L_0^2 / 2 + C_1 L_0}{EI} \tag{18}$$

Stage 3: ($M_y < M_{r1} \le M_u$ and $M_y < M_0 \le M_u$)

In this stage, the two cantilever beams begin to rotate relative to each other, once their end moments have reached their yield values. H and L_0 are still calculated using Equations (14) and (17), respectively. F and C_1 are obtained from Equations (19) and (20), respectively. Once these parameters are updated, the vertical deformation

$\delta_{1,end}$ can be obtained from Equation (18).

$$F = \frac{(M_0 + M_y)EI - HM_0L_2^2/2 + (K_r + HL_0)\left[2(M_0 - M_y)EI/K_r - HL_2^2/2 + M_0(L_0 + L_2)\right]}{EIL_0 - HL_0^3/6 + K_rL_0^2/2} \tag{19}$$

$$C_1 = 2(M_0 - M_y)EI/K_r - \frac{1}{2}FL_0^2 - \frac{1}{2}HL_2^2 + M_0(L_0 + L_2) \tag{20}$$

Stage 4: ($M_{r1} = M_u$ and $M_y < M_0 \leq M_u$)

In this stage, F and C_1 are updated using Equations (22) and (23), respectively, and L_0 is still iteratively calculated using Equation (17). The vertical deformation $\delta_{1,end}$ can be obtained from Equation (21).

$$\delta_{1,end} = \frac{2(M_0 - M_y)EIL_0/K_r - M_uL_0^2/6 + M_0(L_0^2/3 + L_0L_2) - HL_0L_2^2/2}{EI + HL_0^2/6} \tag{21}$$

$$F = (M_U + M_0 + H\delta)/L_0 \tag{22}$$

$$C_1 = \left(EI\delta_{1,end} - FL_0^3/3 + M_0L_0^2/2\right)/L_0 \tag{23}$$

Stage 5: ($M_{r1} = M_u$ and $M_0 = M_u$)

In this stage, both ends of Beam 1 have reached their ultimate moment capacities, and therefore Beam 1 actually rotates as a 'link', as shown in Figure 14 (b). The deformation at the end of Beam 1 can be calculated using Equation (24).

$$\delta_{1,end} = \delta_{1,end} + Ld\theta\cos\theta \tag{24}$$

The mechanical model of a web-cleat connection represented by Equations (10)-(24) has been incorporated into Vulcan following the same methodology as for the novel connection element. Equations (8) and (9) are used to calculate the tangent stiffness matrix of the web-cleat connection element. The Vulcan web-cleat connection element was verified against Abaqus using a single beam model with web-cleat connections at both ends. Temperatures of the web-cleat connections were assumed to be half of that of the connected beam. The mid-span deflection and the axial force of the beam, as obtained by Vulcan and Abaqus, are compared in Figure 15. In general, the Vulcan results are in accordance with those of Abaqus, which indicates that the component-based web-cleat connection element adequately represents the behaviour of web-cleat connections.

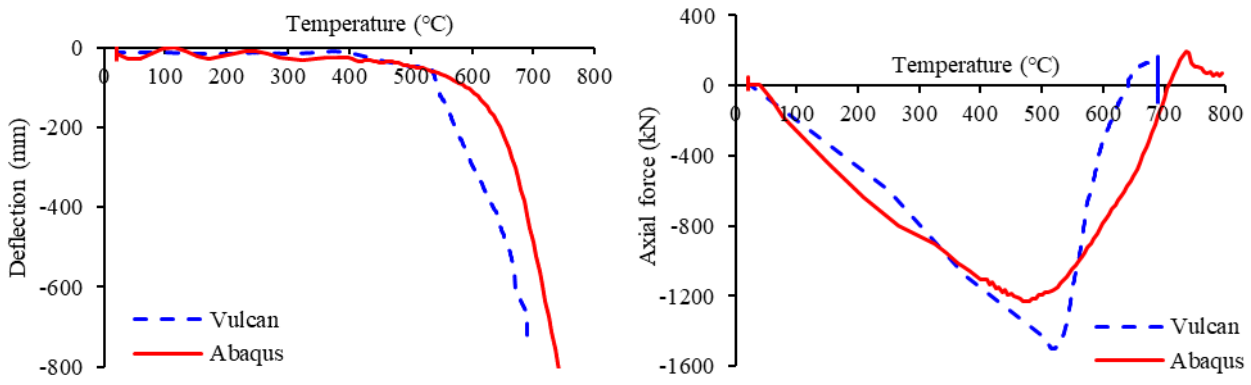

(a) Mid-span deflection of beam (b) Axial force of beam

Figure 15. Comparison results to validate the web-cleat connection element

4.2 Comparison of the novel connection with other connection types

After incorporating the web-cleat connection element in Vulcan, sub-frame models of the geometry shown in Figure 13 (a) were created, using different types of connection. It is assumed that fire occurs on the first floor of the sub-frame, and that temperatures of the lower columns and connections are half of that of the beam, whereas the upper columns stay at ambient temperature. Five different types of connection were selected, including the novel connection, idealised rigid and pinned connections, and conventional end-plate and web-cleat connections. The dimensions of the ductile, end-plate and web-cleat connections (the latter two designed according to Eurocode 3 Part 1-1 [26]) are shown in Figures 4, 13 (b) and 13 (c), respectively. It should be noted that the end-plate and web-cleat connections have the same key dimensions as the ductile connection, including the thickness, the width and the depth of the plate, as well as their bolt spacing, to ensure comparability. The behaviour of the beam using these different end connections is compared in Figure 16 to Figure 18.

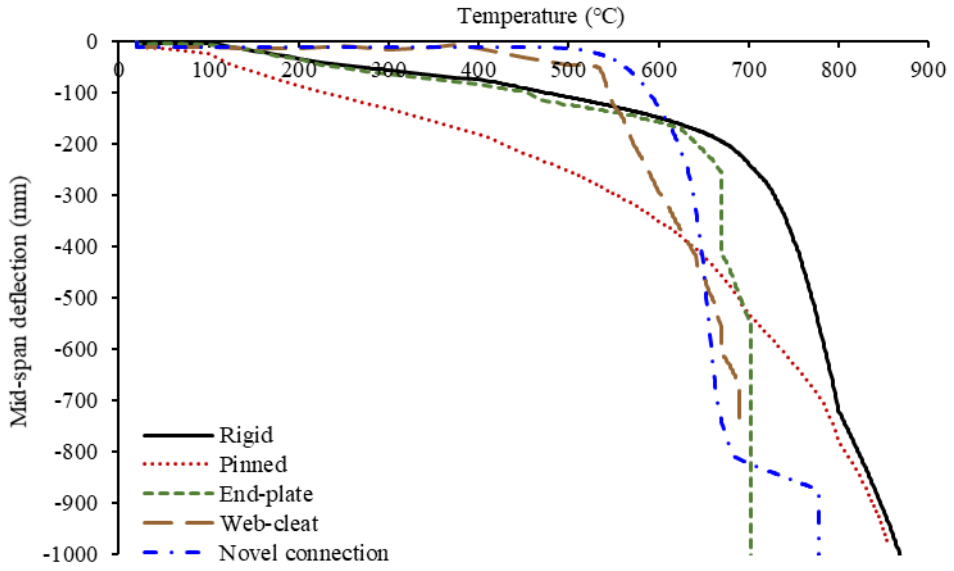

Figure 16. Mid-span deflection of beams with various end connections

As shown in Figure 16, the mid-span deflection of the beam with the novel connections is very close to that of the beam with web-cleat connections. The rotations at the beam ends with the novel connections are much higher than those with end-plate and web-cleat connections (Figure 17). The axial force generated in the beam with the novel connections is very significantly reduced compared to those with all the other connection types, as shown in Figure 18. These phenomena indicate that the novel connection provides much higher axial and rotational ductilities, which successfully accommodate the deformations generated by the connected beams as their temperatures rise. As part of this process, these connections are instrumental in greatly reducing the axial forces to which the surrounding structure is subjected. The failure temperature of the novel connection under the tensile axial forces generated by the eventual catenary action of the heated beams at high temperatures is much higher than that of end-plate and web-cleat connections. This performance could be further improved by optimizing the design of the novel connection, which will be described in the next section.

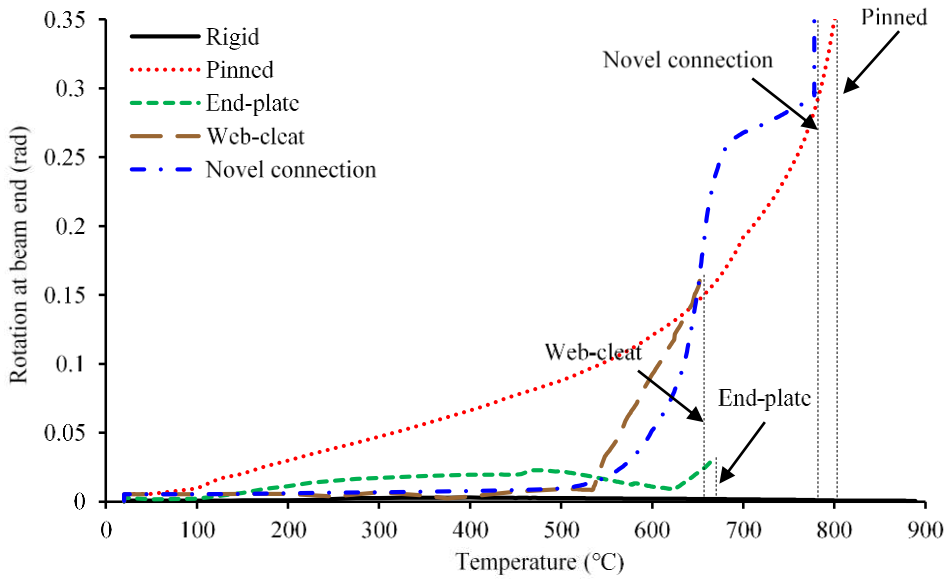

Figure 17. Rotations at beam ends for different connection types

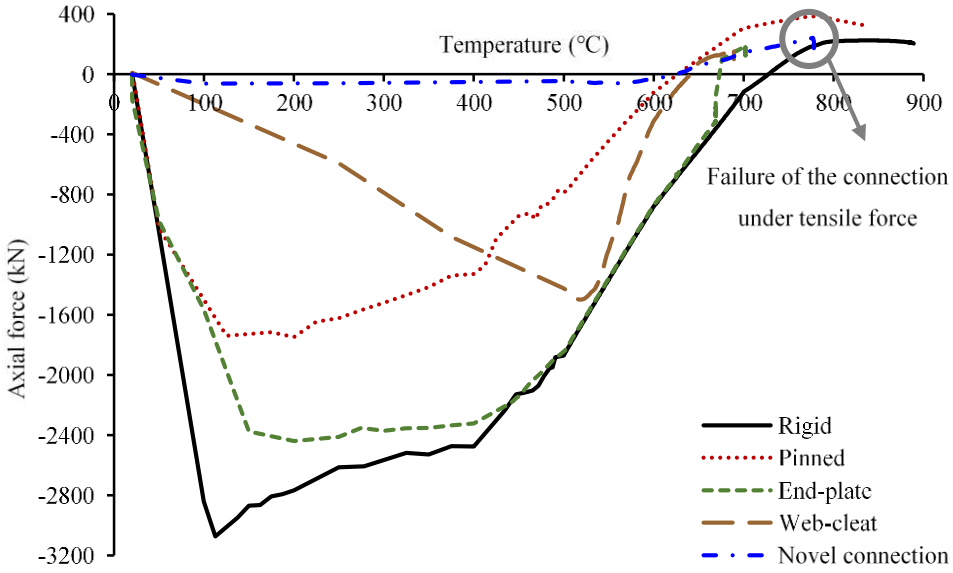

Figure 18. Axial forces of beams with different end connection types

5. Optimization of the novel connection design

In this section, parametric studies are carried out on several key parameters, using the sub-frame shown in Figure 13 (a), to optimize the design of the novel connection in terms of the beam's failure temperature.

It is generally assumed in these studies that the temperature of the connection is equal to half of that of the connected beam in the model used in Section 4. Connections tend to experience lower temperatures than the

members which they connect during a fire event, due to their greater massivity, lower exposed surface area, and fire protection measures which tend to imitate those of the attached column. A sensitivity analysis has been conducted, adopting different relationships between the connection temperature and the beam temperature. The results are shown in Figure 19 and Table 1. The beam temperature at which the connection fails is increased by 13.9% when its temperature is reduced to 40% of the beam temperature. Further reductions of the connection temperature ratio have little effect on increasing the failure temperature of the beam. This is due to the fact that the temperature of the connection will not exceed 400 ℃ if it is assumed to be lower than 40% of the beam temperature. Therefore, it is a reasonable choice to protect the connection to prevent its temperature exceeding 40% of the beam temperature. Further reducing the connection temperature will only increase the cost of insulation to the connection.

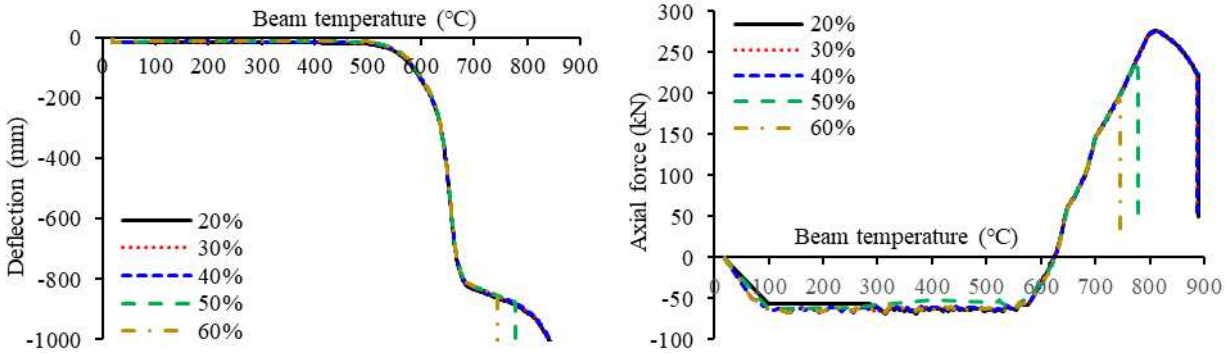

(a) Mid-span deflection of beam (b) Axial force of beam

Figure 19. The effect of different temperature ratio assumptions

Table 1. Beam failure temperatures under different temperature ratio assumptions

Connection temperature ratio	Beam failure temperature (°C)	Difference from original design
$T_C = 20\%T_B$	889	14.3%
$T_C = 30\%T_B$	887	14.0%
$T_C = 40\%T_B$	886	13.9%
$T_C = 50\%T_B$*	778	0.0%
$T_C = 60\%T_B$	745	-4.2%

* Control case

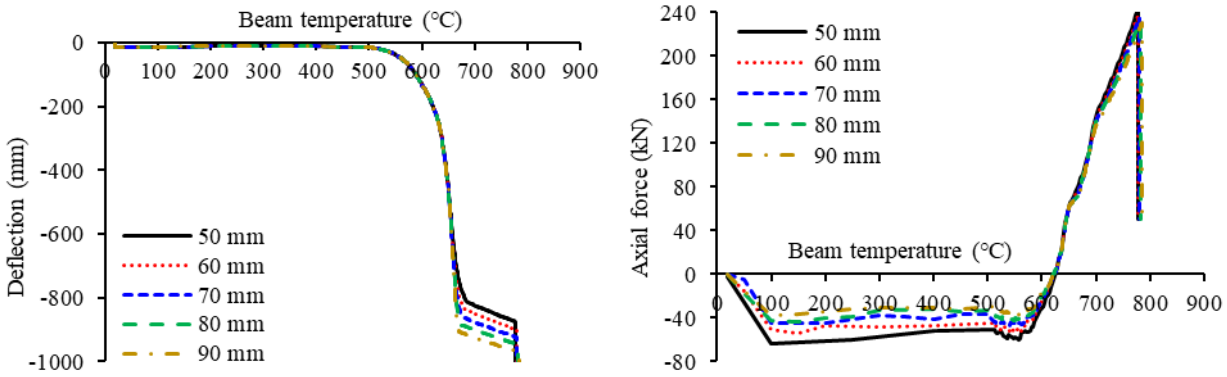

(a) Mid-span deflection of beam (b) Axial force of beam

Figure 20. The effect of changing the inner radius of the semi-cylindrical section

Table 2. Beam failure temperatures with different inner radii of the semi-cylindrical section

Inner radius (mm)	Beam failure temperature (°C)	Difference from original design
50*	778	0.0%
60	779	0.1%
70	781	0.4%
80	782	0.5%
90	785	0.9%

* Control case

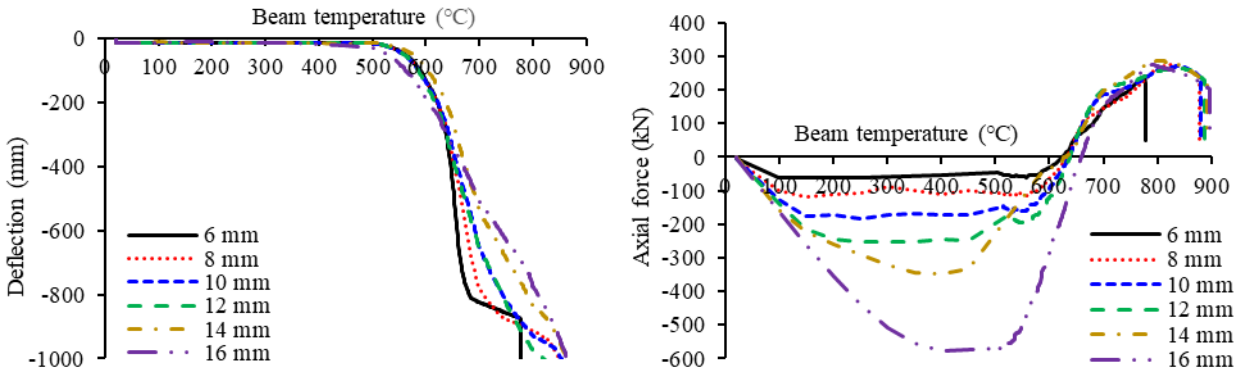

(a) Mid-span deflection of beam (b) Axial force of beam

Figure 21. The effect of changing the plate thickness of the connection

Table 3. Beam failure temperatures with different connection plate thickness

Plate thickness (mm)	Beam failure temperature (°C)	Difference from original design	Maximum compressive axial force (kN)	Difference from original design

6*	778	0.0%	-59.75	0.0%
8	878	12.9%	-116.48	94.9%
10	881	13.2%	-183.54	207.2%
12	888	14.1%	-253.01	323.4%
14	894	14.9%	-346.81	480.4%

* Control case

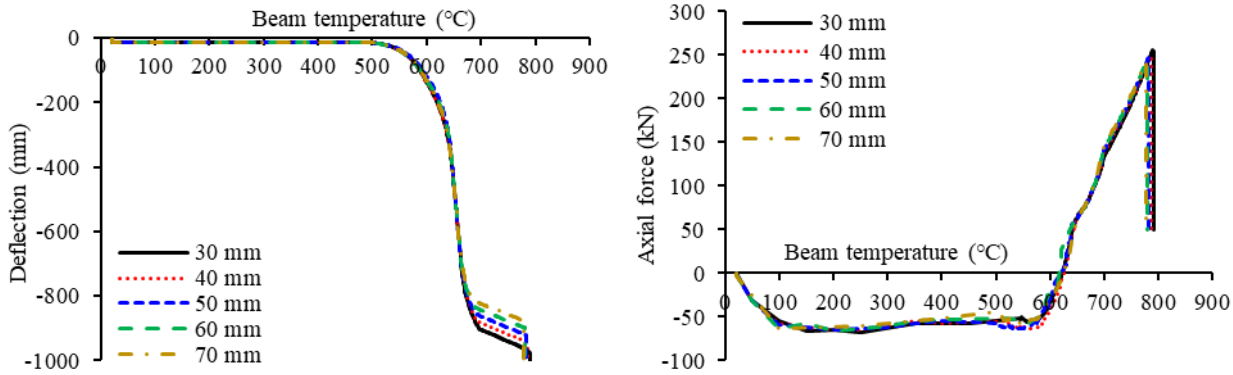

(a) Mid-span deflection of beam (b) Axial force of beam

Figure 22. The effect of different vertical bolt spacing

Table 4. Beam failure temperatures with different vertical bolt spacing

Bolt spacing (mm)	Beam failure temperature (°C)	Difference from original design
30	791	1.7%
40	786	1.0%
50	783	0.6%
60	780	0.3%
70*	778	0.0%

* Control case

In the component-based connection element, if the axial force of a spring row reaches the failure load of the bolt pull-out component, then the spring row is judged to have failed. Therefore, the occurrence of bolt pull-out failure can be delayed by reducing the axial force generated in each spring row. This can be achieved by improving the ductility of the connection, typically by increasing the radius of the semi-cylindrical section. Another way to increase the failure load of the bolt pull-out component is to increase the thickness of plate. The top bolt row experiences the largest tensile displacement when the connection is subject to positive rotation. Moving from the

top bolt row towards the bottom one, the tensile displacement of each bolt row decreases progressively. In order to reduce the maximum tensile displacement, in the top spring row, reducing the vertical bolt spacing could also be effective. Therefore, various inner radii of the semi-cylindrical section, plate thicknesses and bolt spacings have been adopted. The effects of these variations on the mid-span deflection and the axial force of the beam are shown in Figures 20 - 22 and Tables 2 - 4. As shown in Figure 20 and Table 2, increasing the radius of the semi-cylindrical section can reduce the axial compressive force generated in the beam. However, its effect on the maximum tensile force of the beam in catenary action, and the final beam failure temperature, is negligible. For instance, even when the inner radius of the semi-cylindrical section is increased to 90mm, the beam failure temperature is only 0.9% higher than the control case (inner radius of semi-cylindrical section = 50mm). Increasing the plate thickness can significantly improve the performance of the connection in the catenary tension stage, by enhancing the ultimate failure temperature, as shown in Figure 21 and Table 3. However, the increase of plate thickness also reduces the ductility of the connection, resulting in larger axial forces generated in the connected beam. For example, the beam failure temperature with a connection of 10 mm thickness is 13.2% higher than that of the control case, whereas the maximum compressive axial force increases by 207.2% during the initial heating. Therefore, the plate thickness should not be increased excessively, otherwise, the ductility of the connection will decrease sharply, and this may impose very high forces on adjacent structure. Figure 22 and Table 4 show that the bolt spacing has little influence on the ultimate failure temperature of the connection. In order to test the effectiveness of the connection optimization, a ductile connection of 8 mm thickness is adopted in the sub-frame model shown in Figure 13 (a). The inner radius of the semi-cylindrical section is 70 mm, the temperature of the connection is assumed to be 40% of that of the connected beam, and the vertical bolt spacing is 50mm. Figure 23 shows that the optimized ductile connection delivers a much higher failure temperature compared with the original design of the ductile connection (inner radius = 50mm, plate thickness = 6mm, bolt spacing = 70mm, connection temperature = 50% of beam temperature), as well as with the end-plate and web-cleat connections.

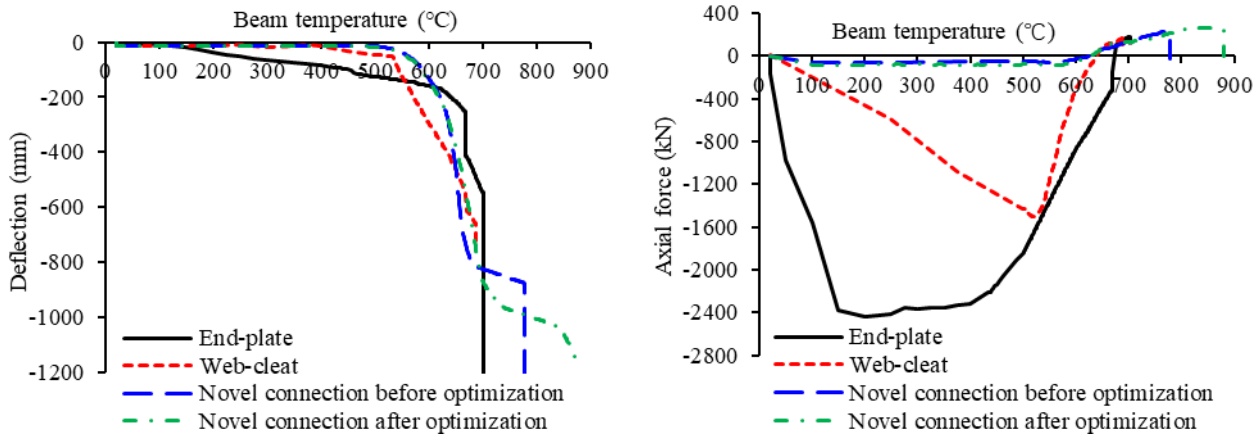

(a) Mid-span deflection of beam

(b) Axial force of beam

Figure 23. Comparison of beam performance with different connection details.

6. Progressive collapse modelling

Once a connection fractures, the connected beam can be detached from the supporting column, leading to an increase in the column slenderness, which might cause the column to buckle. Connection failures can also trigger the collapse of slabs and the spread of fire into adjacent compartments. These may lead to a sequence of failures resulting in the progressive collapse of the entire structure. In order to effectively model the global behaviour of structures in fire from local instability to overall collapse, a combination of static and dynamic solvers was developed by Sun [21-23] and implemented in Vulcan. The static solver is computationally efficient and is used to track the static behaviour of a structure. Once local instability occurs, the dynamic solver is activated to track the motion of the structure until stability is regained, and then the static solver comes back into service. These two solvers are used alternately to analyse the structure under stable and unstable states, respectively. In this section, the static-dynamic solver is used to model the three-storey three-bay plane frame with ductile connections shown in Figure 24, to illustrate the progressive collapse of a structure in fire. Although this model is for a non-composite frame, the contributions of the slabs are considered to some extent: 1) the restraint to the beam top flange given by the slab is considered by constraining the out-of-plane DoFs of the frame; 2) the transfer of external loads from the slab to the beam is considered by directly converting the external loads into UDL and applying onto the beam. It is further assumed that fire occurs only in the ground floor, and the horizontal springs on the outer columns of each floor are used to prevent lateral sway instability of the frame. Only half of the frame is built in the Vulcan model, in order to save computational effort, given that the structure is symmetric. A uniformly distributed line load is applied to the beam on each floor, generating a load ratio of 0.4, with respect to a simply supported beam. A

concentrated vertical force of 3000 kN is applied on each of the two intermediate columns, representing superstructure loads. The temperatures of the connections and columns at ground floor level are assumed to be half of that of the connected beams.

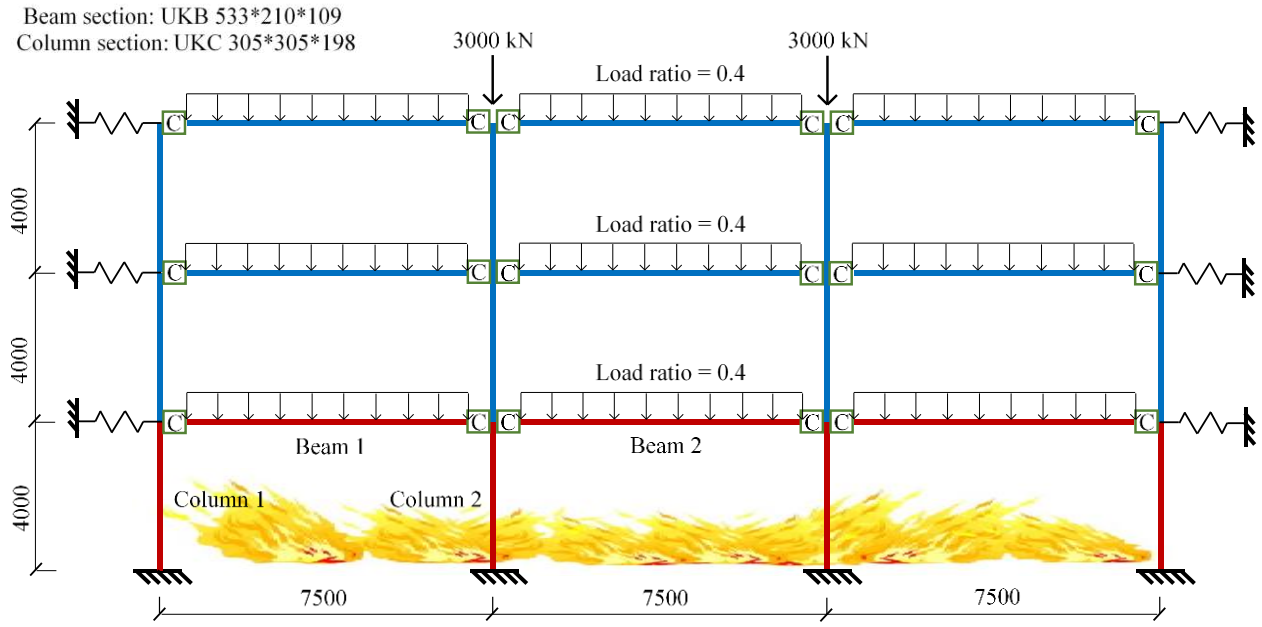

Figure 24. The three-storey three-bay frame

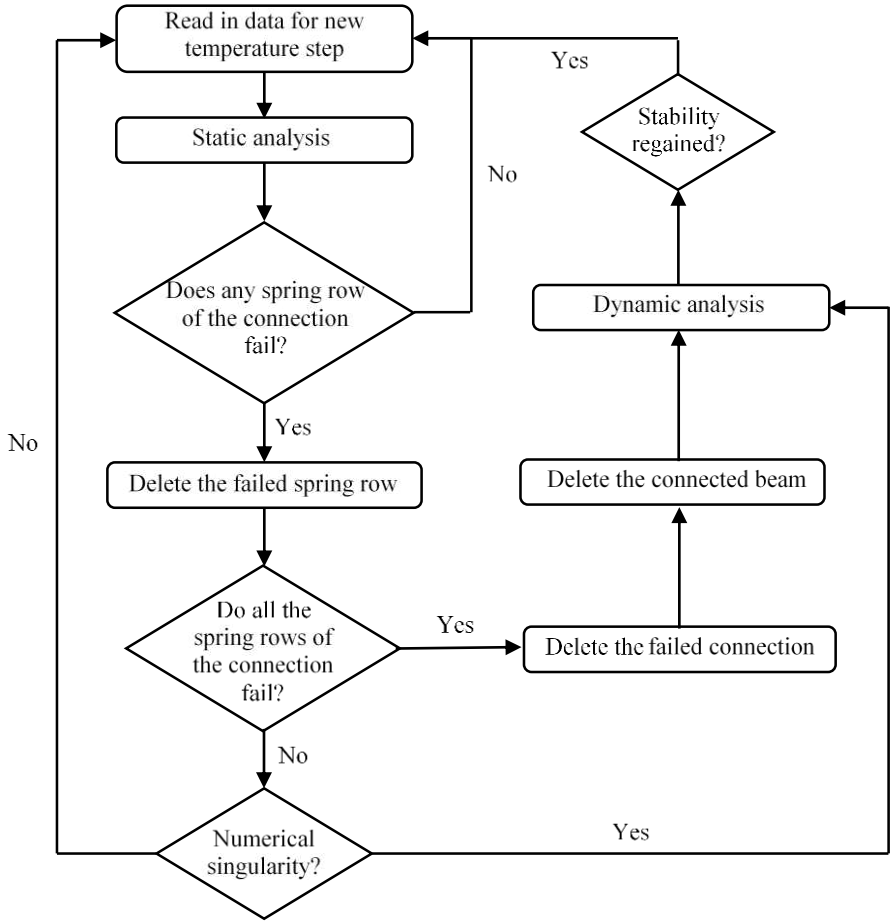

Figure 25. Static-dynamic calculation process

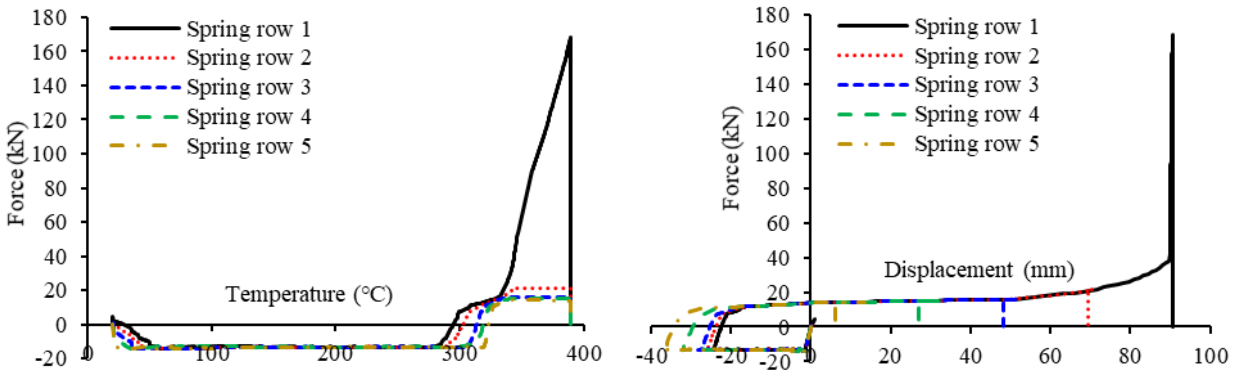

(a) Force-temperature curve of each spring row (b) Force-displacement curve of each spring row

Figure 26. Variation of spring row forces of the connection at the end of Beam 2

The calculation procedure for progressive collapse of the frame is shown in in Figure 25. Firstly, input data is read in for a new temperature step. The static solver is used to analyse the model. As soon as one component of a spring row reaches its failure limit, this spring row is considered as failed, and is deleted. When all spring rows in a connection element fail, the connection is considered as failed, and its stiffness matrix is set to zero. Once both

connections have failed, the connected beam detaches from the columns. It is then removed from the model by restraining all its degrees of freedom. Figure 26 shows temperature-force and displacement-force curves of the spring rows of the connections at the ends of Beam 2. Spring Row 1 (the top bolt row) undergoes the minimum compressive displacement and maximum tensile displacement, whereas Spring Row 5 (the bottom bolt row) undergoes the maximum compressive displacement and minimum tensile displacement. The force-displacement curve of Spring Row 1 becomes almost vertical as failure occurs. However, the tensile capacity of the spring row cannot be reached because its failure is governed by bolt pull-out. Fortunately, several measures discussed in Section 5 can be taken to delay the occurrence of bolt pull-out failure, so as to increase the ultimate failure temperature of the beam. In the novel connection element, once a spring row fails, the force of this spring row falls to zero. The sequence of failures of the other bolt bows follows very closely, once the top bolt bow has pulled out at around 390 °C. Once all the bolt rows have failed, the entire connection is considered as having failed. As can be seen from the progressive collapse of the frame in Figure 27 (b), the connections at the ends of Beam 1 and Beam 2 fail when the beam temperature is 780 °C, and then Beam 1 and Beam 2 are deleted from the frame (Figure 27 (c)). After that, Column 1 and Column 2 continue to be heated, although it is assumed in this case that their upper continuations remain cool, until both of their temperatures reach 550 °C, at which point Column 2 begins to buckle due to the increase of its slenderness ratio. Column 1 does not buckle because of its lateral restraint (Figure 27 (d)-(f)). The progressive collapse simulation of the frame presented in this section emphasizes the importance of connections for the survival of the entire structure in a fire event.

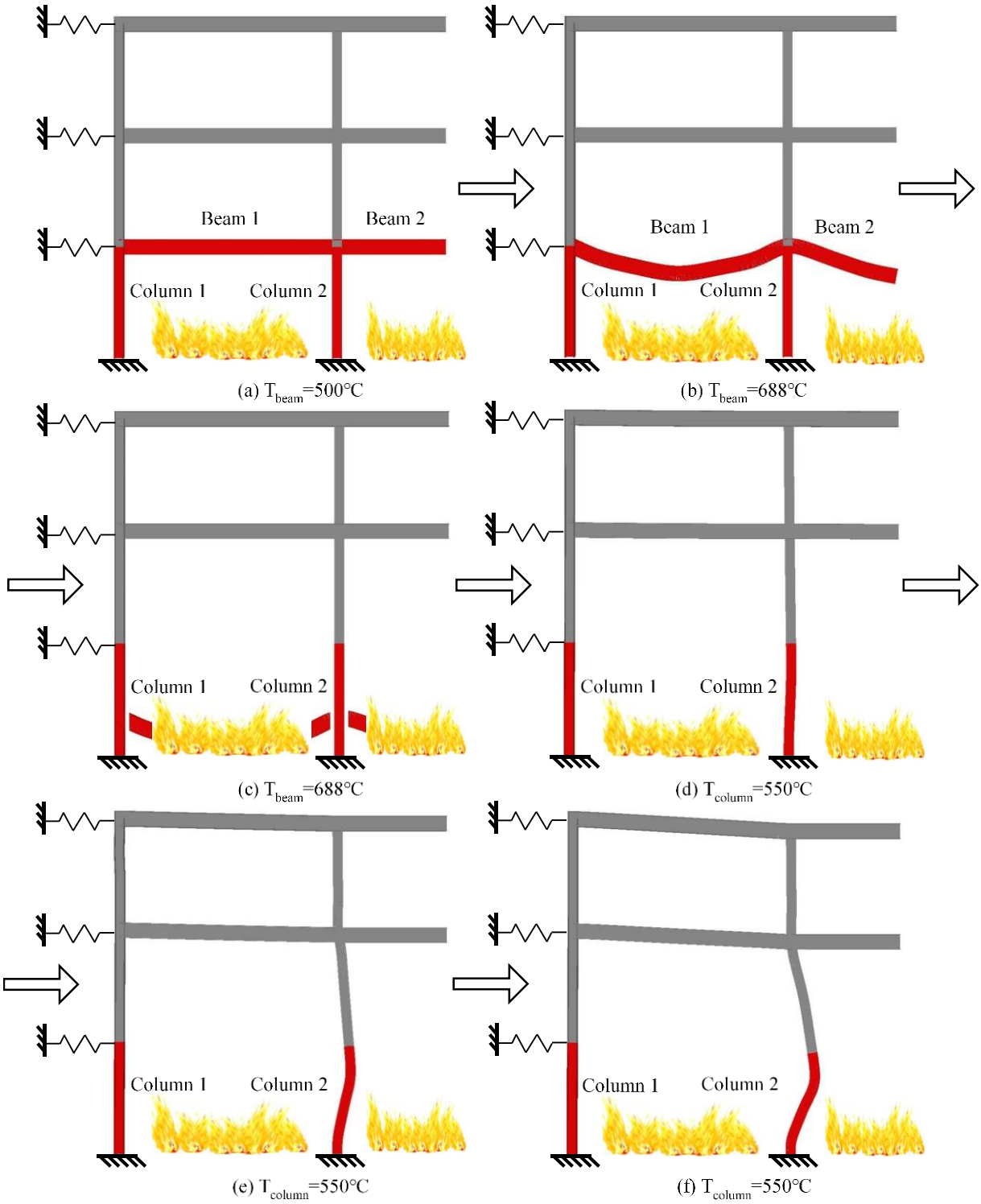

Figure 27. Progressive collapse of the frame

Conclusion

This paper has described the incorporation of a novel connection element into the software Vulcan. The bolt pull-out components, represented by the analytical model developed by Dong [16], have been added to the component-based model of the novel connection to simulate bolt pull-out failure. The tangent stiffness matrix equations derived by Block [13] have been used to convert the component-based model into a connection element following the principles of the finite element method.

A single beam model with novel connections at both its ends was modelled using both Vulcan and Abaqus. It was assumed that there were three cases, in which the temperature of the connection was equal to 20°C, 50% and 100% of the temperature of the connected beam, respectively. The failure temperatures predicted by Abaqus in Cases 2 and 3 are higher than those predicted by Vulcan, because element fracture is not represented in the Abaqus model. In general, the simulation results obtained by Vulcan are very close to those of Abaqus, which indicates that the connection element can adequately represent the behaviour of the novel connection.

A sub-frame model was used to compare the performance of the novel connection with that of conventional connection types. Different types of connection were used in this sub-frame model, including idealised rigid and pinned connections, and conventional end-plate and web-cleat connections. The analytical model of a web-cleat connection, developed by Yu [24], was implemented in Vulcan, following the same method used for the novel connection element. Results show that, compared with other connection types, the novel connection can provide much higher axial and rotational ductilities to accommodate the deformations generated by the connected beams as their temperatures rise.

Parametric studies were carried out to optimize the performance of the novel connection under the tensile axial forces generated by the eventual catenary action of the unprotected beams at high temperatures. Four key parameters including the temperature of the connection, the inner radius of its semi-cylindrical section, the plate thickness and the bolt spacing were selected. It was found that it is possible to optimize connection thickness, protection level, and inner radius of the semi-cylindrical section in order to delay the occurrence of bolt pull-out failure, and thus enhance a beam's ultimate failure temperature.

The static-dynamic solver in Vulcan was used to simulate the progressive collapse of a three-storey three-bay frame with novel connections. It was found that failure of all the spring rows of the heated connection is triggered

by the initial failure of the top bolt-row at a certain temperature. When the connection was judged to have failed the connected beam was then removed from the model. A column previously connected to the deleted beam will eventually buckle due to the increase of its slenderness ratio. This progressive collapse simulation emphasizes the importance of connections for the survival of the entire structure in a fire event.

References

[1] McAllister T, Corley G. World Trade Center Building performance study: Data collection, preliminary observations, and recommendations: Federal Emergency Management Agency; 2002.

[2] Newman GM, Robinson JT, Bailey CG. Fire safe design: A new approach to multi-storey steel-framed buildings: Steel Construction Institute; 2000.

[3] Liu Y, Huang S-S, Burgess I. Investigation of a steel connection to accommodate ductility demand of beams in fire. Journal of Constructional Steel Research. 2019;157:182-97.

[4] Liu Y, Huang S, Burgess I. Ductile connections to improve structural robustness in fire. Proceedings of the 6th Applications of Structural Fire Engineering Conference (ASFE'19): Sheffield; 2019.

[5] Liu Y, Huang S-S, Burgess I. Component-based modelling of a novel ductile steel connection. Engineering Structures. 2020;208:110320.

[6] Yu H, Burgess I, Davison J, Plank R. Numerical simulation of bolted steel connections in fire using explicit dynamic analysis. Journal of Constructional Steel Research. 2008;64:515-25.

[7] Sarraj M, Burgess I, Davison J, Plank R. Finite element modelling of steel fin plate connections in fire. Fire Safety Journal. 2007;42:408-15.

[8] Elsawaf S, Wang Y, Mandal P. Numerical modelling of restrained structural subassemblies of steel beam and CFT columns connected using reverse channels in fire. Engineering Structures. 2011;33:1217-31.

[9] Tschemmernegg F, Tautschnig A, Klein H, Braun C, Humer C. Zur nachgiebigkeit von rahmenknoten–Teil 1. Stahlbau. 1987;56:299-306.

[10] CEN. Eurocode 3: Design of steel structures, Part 1–2: General rules—Structural fire design. BS EN 1993-1-2: 2005. 2005.

[11] Jaspart J-P. General report: session on connections. Journal of Constructional Steel Research. 2000;55:69-89.

[12] Leston-Jones LC. The influence of semi-rigid connections on the performance of steel framed structures in fire [PhD thesis]: University of Sheffield; 1997.

[13] Block FM. Development of a component-based finite element for steel beam-to-column connections at elevated temperatures [PhD thesis]: University of Sheffield Sheffield, UK; 2006.

[14] Spyrou S. Development of a component based model of steel beam-to-column joints at elevated temperatures: University of Sheffield; 2002.

[15] Dong G, Burgess I, Davison B, Sun R. Development of a general component-based connection element for structural fire engineering analysis. Journal of Structural Fire Engineering. 2015;6:247-54.

[16] Dong G. Development of a General-Purpose Component-based Connection Element for Structural Fire Analysis: University of Sheffield; 2016.

[17] Taib M, Burgess I. A component-based model for fin-plate connections in fire. Journal of Structural Fire Engineering. 2013;4:113-22.

[18] Huang Z, Burgess I, Plank R, VULCAN, REISSNER M, Engineers-Structures BJPotIoC et al. THREE-DIMENSIONAL MODELLING OF TWO FULL-SCALE, FIRE TESTS ON A COMPOSITE BUILDING. 1999;134:243-55.
[19] Huang Z, Burgess IW, Plank RJJSJ. Nonlinear analysis of reinforced concrete slabs subjected to fire. 1999;96:127-35.
[20] Huang Z, Burgess IW, Plank RJJJose. Three-dimensional analysis of reinforced concrete beam-column structures in fire. 2009;135:1201-12.
[21] Sun R, Huang Z, Burgess I. Progressive collapse analysis of steel structures under fire conditions. Engineering Structures. 2012;34:400-13.
[22] Sun R, Huang Z, Burgess I. The collapse behaviour of braced steel frames exposed to fire. Journal of Constructional Steel Research. 2012;72:130-42.
[23] Sun RR. Numerical modelling for progressive collapse of steel framed structures in fire [PhD thesis]: University of Sheffield; 2012.
[24] Yu H, Burgess I, Davison J, Plank R. Tying capacity of web cleat connections in fire, Part 2: Development of component-based model. Engineering structures. 2009;31:697-708.
[25] Yu H, Burgess I, Davison J, Plank R. Tying capacity of web cleat connections in fire, Part 1: Test and finite element simulation. Engineering Structures. 2009;31:651-63.
[26] Institution LBS. BS EN 1993-1-8, “Eurocode 3: Design of steel structures: Part 1-8, Design of joints” 2005;18.